

Hydrogen and Helium Plasmas in the GOLEM Tokamak

George Sarancha^{1,2}, Alexey Drozd^{1,3}, Stanislav Ganin^{1,3}, Daniela Kropachkova⁴, Ivan Kudashev^{1,3}, Vladimir Kulagin^{1,3}, Martina Lauerova⁴, Alexander Melnikov^{1,2,3}, Nikita Sergeev^{1,3}, Oleg Krokhaliev^{1,2}, Jan Stockel⁴ and Vojtech Svoboda⁴

¹ National Research Center “Kurchatov Institute”, Moscow, Russian Federation

² Moscow Institute of Physics and Technology (National Research University), Dolgoprudny, Moscow region, Russian Federation

³ National Research Nuclear University “MEPhI”, Moscow, Russian Federation

⁴ Faculty of Nuclear Sciences and Physical Engineering, Czech Technical University in Prague, Czech Republic

E-mail: sarancha.ga@phystech.edu

Abstract

The helium plasma properties and confinement remain an important area of research in modern fusion devices. This work is dedicated to the helium plasma initiation and control in a small-scale tokamak GOLEM compared to hydrogen plasma. Helium and hydrogen plasmas are comprehensively compared and the optimum operational conditions for the start-up are found. Long-range correlations between low-frequency (< 50 kHz) electrostatic and magnetic oscillations are found, as well as broadband (< 250 kHz) magnetic oscillations resolved in frequency and wave vector in helium plasma.

1. Introduction

Experiments with helium plasma are quite unique in modern fusion devices. They are mostly made on large scale devices and dedicated to ITER relevant studies for non-nuclear phase of operation. Helium plasma performance is always lower than hydrogen or deuterium ones with identical plasma current I_{pl} , toroidal magnetic field B_t , line-averaged electron density \bar{n}_e and heating power [1]. It was shown that energy confinement time for helium plasmas are about 30% lower than for deuterium ones. This reduced plasma confinement, contradicting to gyro-Bohm scaling, might be coupled to the isotope effect suggesting better confinement for the isotope with larger mass. Several theoretical mechanisms including $E \times B$ shearing [2, 3] and collisional effects [4] were proposed explain this effect but there is no satisfactory explanation so far.

To expand the experimental database for helium plasma confinement properties, it will be helpful to investigate its operational domain from large machines to small-scale ones with low electron temperature and plasma density.

Small and medium-size fusion devices could be of a great support for the mainstream plasma research in various topics [5, 6, 7]. This research is coordinated by IAEA Coordinated Research Program (CRP) with a participation of the GOLEM tokamak [8], formerly CASTOR [9, 10]. In addition to the research tasks the teaching and the training of the young plasma physicists becomes an essential element of the CRP [11].

The experiments aimed at learning the basics of helium plasma confinement were performed remotely in GOLEM by a team of graduate students of National Research Nuclear University MEPhI and National Research University MIPT as a part of the course “Technology of the thermonuclear experiment”.

Special attention is paid to the gas breakdown process and its comparison for hydrogen and helium discharges. For this study, a series of discharges with vacuum vessel pre-cleaning have been produced. Hydrogen and helium plasmas were studied with identical pre-selected discharge setup parameters allowing the detail comparison.

In addition, the study is focused to the electrostatic and magnetic turbulence and their correlation properties. Long-range correlations are characteristic features of the Zonal Flows – a mechanism of the broadband turbulence self-regulations [1, 12]. Zonal Flows and their higher frequency counterpart Geodesic Acoustic Modes were recently studied in tokamaks [13, 14, 15] and stellarators [16, 17, 18, 19] of small and medium size. Search of the Zonal Flows in the GOLEM tokamak could be one of the most important contributions to the mainstream fusion research.

2. The GOLEM tokamak

GOLEM tokamak has a circular cross section with the major/minor radius $R = 0.4$ m, $a = 0.1$ m [20]. After upgrades the circular stainless-steel vessel was equipped with a molybdenum poloidal limiter located at radius $a_{lim} = 0.085$ m. Due to the origin of the machine whole vacuum chamber is surrounded by copper shell. The power supply system is based on the capacitor banks. Each of the individual winding, including central solenoid, is connected to the separated capacitor banks, which allows to easily adjust the desired value of current passing through the coils. GOLEM has a unique capability of the remote control via Internet [21].

Before plasma experiment, the vacuum vessel was carefully conditioned by inductive heating for up to 200°C for 60 min, which was followed by a cleaning glow discharge in order to remove impurities from the vacuum vessel. Glow discharge cleaning has gas pressure around 1 Pa, duration 20 min., and the discharge current about 0.5 A. Glow discharge was made with the working gas, hydrogen for H-plasmas, helium for He-plasmas. Such treatment results in the background gas pressure as low as 0.1 mPa.

GOLEM gas control system has no option for active gas puffing during the shot, so the experimental data discussed here are performed in Ohmic discharges with no density control. For easy plasma start-up, in view of difference of the ionization energy for hydrogen and helium gases, pre-ionization by an electron gun was conventionally used.

Present experiments were performed for helium and hydrogen with plasma current $I_{pl} = 2.5$ -3.0 kA, line-averaged density $\bar{n}_e = 5 \cdot 10^{17} \text{ m}^{-3}$ and toroidal magnetic field $B_t = 0.22$ T.

3. Diagnostics on GOLEM

The machine is equipped with set of standard diagnostics [22], which are capable to measure the loop voltage U_{loop} , plasma current I_{pl} , toroidal magnetic field B_t and visible light emission measurements. For the studies of magnetic oscillations GOLEM is equipped with four Mirnov Coils. Electric probes were used to study the edge plasma parameters.

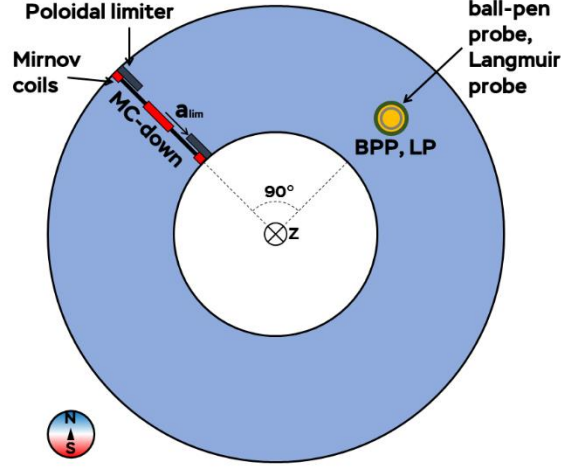


Figure 1. Diagnostic set-up

3.1. Mirnov Coils

Mirnov Coils are used to the plasma position determination on GOLEM. Mirnov Coils (MC) are placed inside the vacuum chamber at the radius $b = 0.093$ m as shown in fig. 1.

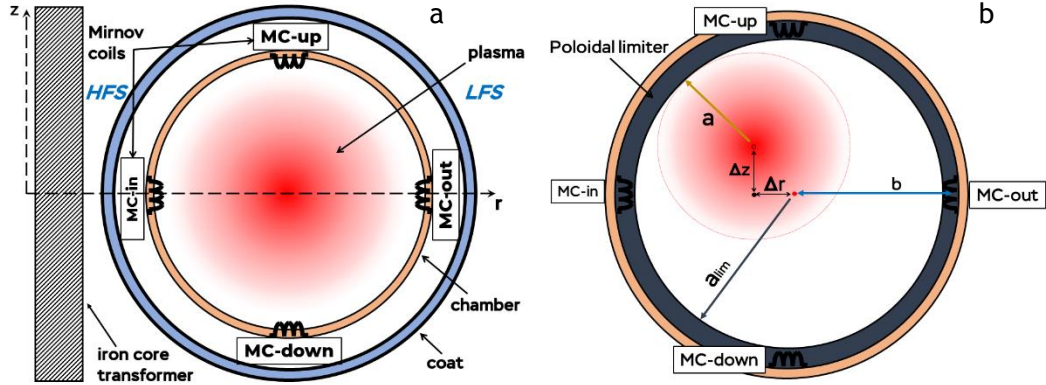


Figure 2. a) in-vessel components including Mirnov Coils; b) schematic for plasma displacement calculation

The effective area of each MC is $A = 3.8 \cdot 10^{-3} \text{ m}^2$. Coils MC-out and MC-in are used to determine the horizontal plasma position and MC-up and MC-down - to determine the vertical plasma position.

The coils measure voltage induced by changes in poloidal magnetic field. To get the absolute value of poloidal magnetic field, one should integrate the measured voltage U and normalize by an effective area:

$$B(t) = -\frac{1}{A} \int_0^t U(\tau) d\tau \quad [T, m^2, V, s]$$

Ideally, axis of the coil is perpendicular to the toroidal magnetic field, but in fact they are slightly deflected so measured signal is contaminated by some amount of toroidal magnetic field. For determination of plasma position this parasitic signal should be removed. Vacuum discharge with the same parameters as plasma discharge is used for this purpose. Mirnov Coils signal in the vacuum discharge has no plasma signal, but only toroidal magnetic field and also some other magnetic fields e.g. generated by poloidal windings. This vacuum signal is subtracted from the active signal from plasma discharge.

Straight conductor approximation is made for calculation of plasma column displacement. With values of poloidal field on the two opposite sides of the column, its horizontal displacement can be expressed as:

$$\Delta r = \frac{B_{MC-out} - B_{MC-in}}{B_{MC-out} + B_{MC-in}} \cdot b \quad [cm, T]$$

and for vertical plasma displacement:

$$\Delta z = \frac{B_{MC-up} - B_{MC-down}}{B_{MC-up} + B_{MC-down}} \cdot b \quad [cm, T]$$

As plasma column is limited by poloidal limiter, for displaced plasma the minor radius a can be calculated as:

$$a = a_{lim} - \sqrt{\Delta r^2 + \Delta z^2} \quad [cm]$$

see figure 2(b).

3.2. Electric probes

The edge plasma parameters are measured by the combined probe head inserted in the GOLEM vessel through the bottom diagnostic port. The probe head is composed by the Ball Pen Probe (BPP) and the single Langmuir Probe located at the same magnetic surface $r_{\text{probe}} = 0.085$ m, equals to a_{lim} . Both probes operate in the floating regime, their signals are recorded via the voltage divider 1:100 with the total resistivity 0.7 M Ω . Ball Pen probe directly measures the plasma potential ϕ_{pl} , as it was shown in [23], and references inside. The Langmuir probe measures the floating potential ϕ_{fl} .

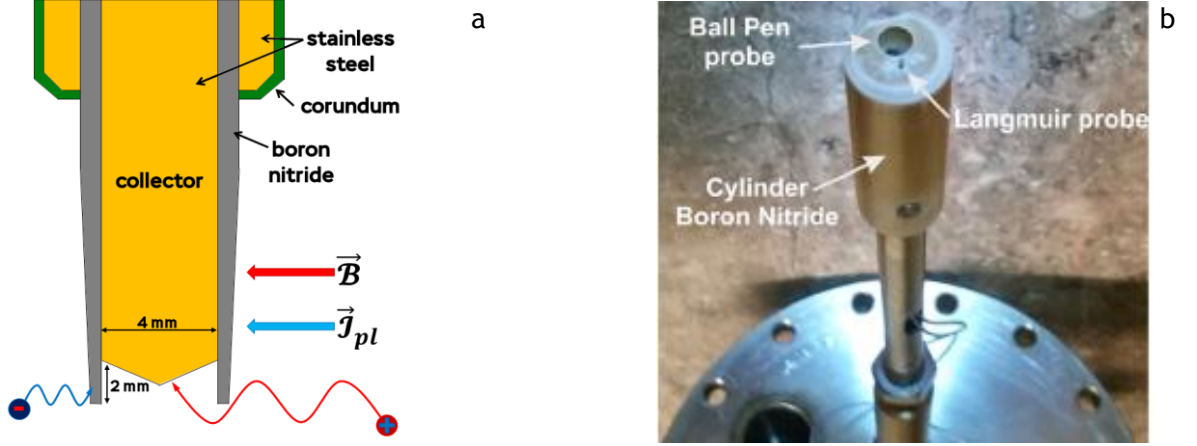


Fig 3. Electric probes. Left – schematic and principle of the Ball Pen probe. The collector is located inside an insulated cylinder by the depth of 2 mm. In this case, the collected electron current is significantly screened because of a smaller electron Larmor radius. Right – photo of the combined probe head

This combined probe head allows determination of the electron temperature by using the expression [24]:

$$T_e = \frac{\phi_{\text{pl}} - \phi_{\text{fl}}}{\alpha} \text{ [eV, V]}$$

The calibration factor α is equal to 2.5 V/eV for hydrogen plasmas and 2 V/eV for helium plasmas for typical toroidal magnetic field of GOLEM. Note that the combined BPP+LP probe head allows T_e measurement with the temporal resolution limited just by the sampling rate of the data acquisition system, which is 1 MSPS.

4. Experimental setup

The present study was performed remotely in *May 2020* with 93 discharges in hydrogen and helium executed during two afternoon experimental sessions:

- 52 discharges with helium plasmas – (##33011–33063)
- 41 discharges with hydrogen plasmas – (##33064–33105)

Experimental data are stored in the GOLEM database and freely available at <http://GOLEM.fjfi.cvut.cz/shots/SHOT#/>.

Machine operation was performed in so-called “basic mode”, when only two capacitor banks were remotely controlled: the first one for the toroidal field coils (U_{B_t}), and the second one for primary winding of the iron core transformer (U_{CD}). The working gas (either hydrogen or helium) and its pressure is preselected. Range of the preset control parameters are presented in the table 1.

Working gas	U_{B_t} [V]	B_t [T]	U_{CD} [V]	$\tau(U_{\text{CD}})$ [ms]	p [mPa]	Pre-ionization by electron gun
H/He	1000	0.2–0.3	400–750	1	10 - 230	ON

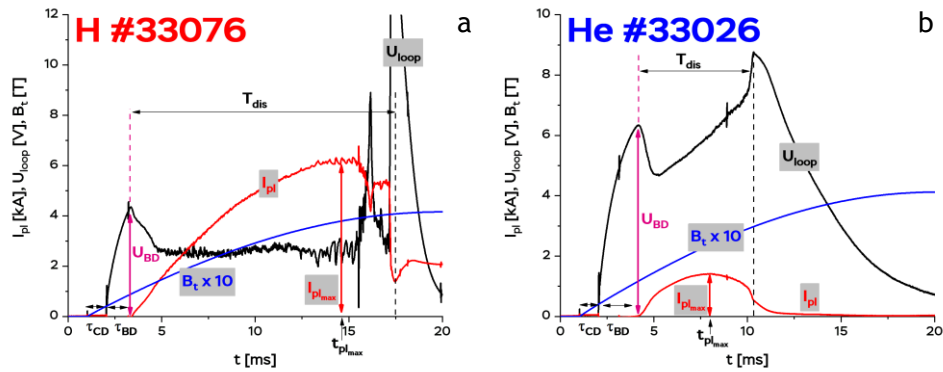


Figure 4. Temporal evolution of the hydrogen (a) and helium (b) discharge parameters.

Discharge scenario for hydrogen and helium plasmas is shown in Figure 4. The data acquisition system collecting all discharge parameters starts at $t = 0$. The toroidal magnetic field starts at $t = 1$ ms and increases in time. After the delay $\tau_{\text{CD}} = 1$ ms, the capacitor bank for powering the primary winding of the transformer is switched on and generates the loop voltage U_{loop} . The

increasing loop voltage accelerates electrons produced by the pre-ionization source and avalanche ionization of the working gas occurs. After some delay, $\tau_{BD} \sim 1-2$ ms, the plasma density becomes sufficiently high, and the plasma breakdown happens and plasma current starts to increase. At that time, the loop voltage reaches a maximum value U_{BD} and then drops dramatically. Later on, the discharge evolves spontaneously, since no control system for plasma current and plasma column displacement is available on GOLEM during this experiment. The discharge terminates by a sharp drop of the plasma current. The time interval between the breakdown time and termination of the plasma current is taken as the discharge duration T_{dis} . The plasma current increases during the discharge and in some moment reaches its maximum, $I_{pl_{max}}$. In this study, we take this time as a reference to compare various experimental plasma parameters. Figure 4 highlights the differences between plasma parameters for the same scenario in hydrogen and helium plasmas.

5. Experimental results

5.1. Breakdown studies

Some features of breakdown on the GOLEM tokamak in hydrogen was studied in [20]. Here we focus on the comparison of breakdown in hydrogen and helium working gas. The time-traces of the main plasma parameters are shown in fig 5.

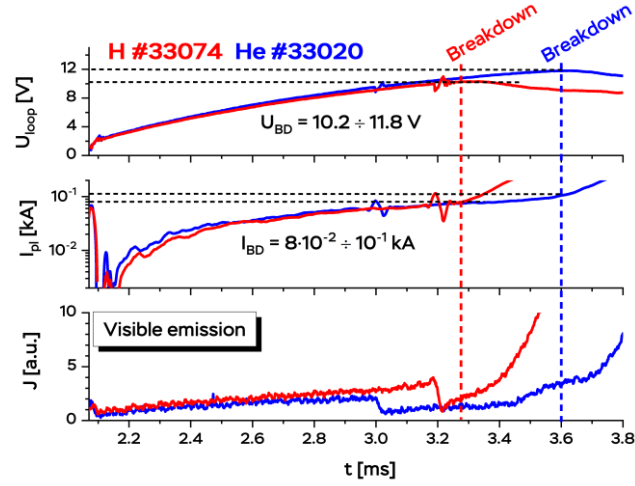


Figure 5. Plasma start-up for two similar discharges executed at $U_{CD} = 500$ V. The working gas pressure is $p_H = 27$ mPa, $p_{He} = 31.5$ mPa. (Fast jumps on all signals at $t = 3.0$ and 3.2 ms appears due to machine power supplies triggers on the GOLEM data acquisition system)

The loop voltage applied at $t = 2.1$ ms causes the electrons acceleration along magnetic field lines by the toroidal electric field $E_t = \frac{U_{loop}}{2\pi R}$ to a drift velocity $v_D \sim \sqrt{\frac{E_t}{p}}$ and p is the gas pressure. Once their energy prevails the ionization energy of the working gas molecules/atoms, the electron density n_e and the plasma current $I_{pl} \sim n_e v_D$ increases. The initial fast increase of I_{pl} is slowed down because of charged particle losses, due to stray magnetic fields and subsequent polarization of plasma column followed by fast convective losses [25, 26]. When $I_{pl} \geq 80-100$ A, its poloidal magnetic field becomes comparable with stray magnetic fields, the particle losses are dramatically reduced, and plasma current starts to increase much faster. The plasma resistivity $R_{pl} \sim \frac{U_{loop}}{I_{pl}} \approx 100$ m Ω , becomes a non-negligible fraction of the resistivity of the GOLEM vessel, $R_v \approx 10$ m Ω . Consequently, the loop voltage starts to decrease.

Fig. 5 shows the similarity in hydrogen and helium plasmas. The only visible difference is a longer avalanche phase in helium and consequent higher breakdown voltage. This might be caused by differences electron drift velocities, gas pressures and first Townsend coefficient in hydrogen and helium. Scaling of the breakdown voltage with the working gas pressure is shown in fig. 6.

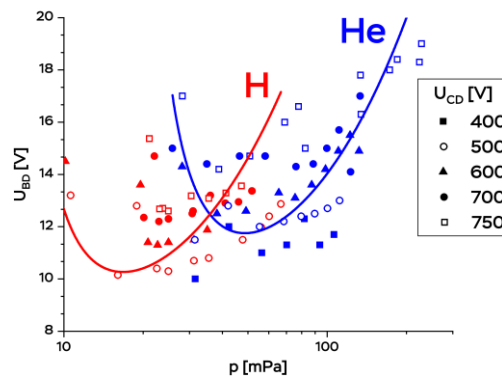


Figure 6. Dependency of the breakdown voltage on the gas pressure for various U_{CD}

The full lines are polynomial fits of all data to guide the eyes. Figure 6 shows that the optimum range of pressures to get the lowest breakdown voltage is between 20 – 50 mPa for both hydrogen and helium, where the breakdown voltage is between 10÷13 V. Note also that the data and in particular fit for hydrogen resemble the Paschen curve $U_{BD} = \frac{A \cdot 2\pi R p}{\ln 2\pi R p + B}$, where A and B are first and second Townsend coefficients.

5.2. Discharge duration

Duration of discharge is an important parameter on GOLEM. It has to be maximized (or optimized) to get sufficiently long time for any physical experiments. Figure 7 compares the discharge duration in hydrogen and helium plasmas.

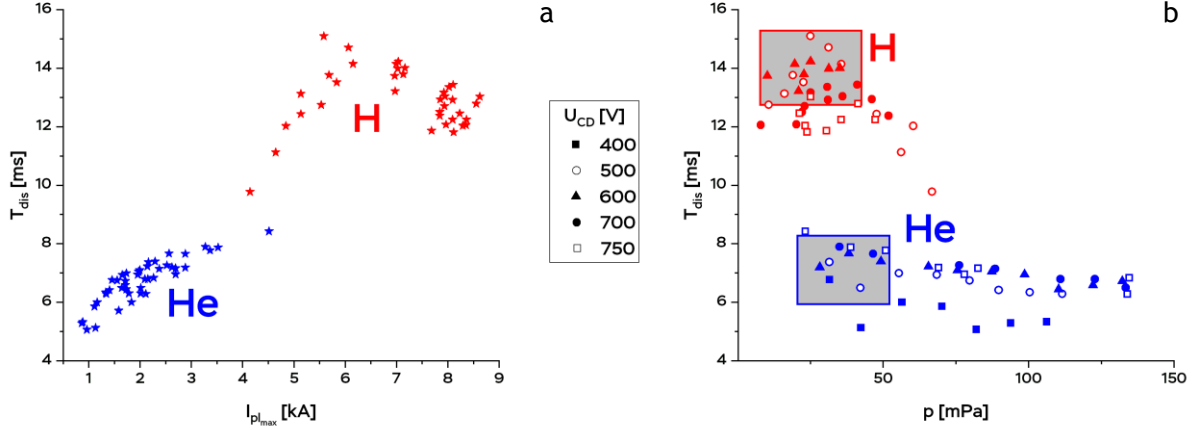


Figure 7. Discharge duration in hydrogen (red symbols) and helium (blue symbols) versus maximum plasma current for all U_{CD} (a) and the gas pressure (b) for various U_{CD}

Experiment shows that discharge duration in hydrogen plasmas is noticeably longer than in helium ones by a factor of 2, and it slightly reduces when the gas pressure increases.

The shadowed rectangular areas show roughly the optimum parameters to achieve longer discharge:

- hydrogen – $p_H = 10 \div 35$ mPa, $U_{CD} = 500 \div 600$ V;
- helium – $p_{He} = 20 \div 50$ mPa, $U_{CD} = 600 \div 750$ V.

5.3. Maximum plasma current

Figure 8 shows the plasma current dependence on the working gas pressure for a various voltages applied to primary winding of the GOLEM transformer U_{CD} .

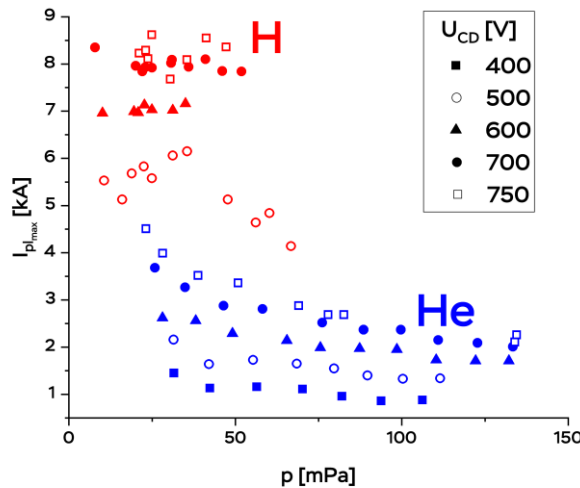


Figure 8. Dependency of the maximum plasma current on the gas pressure for various U_{CD} [V]

We clearly observe decrease of the maximum current $I_{pl_{max}}$ with the pressure in the both H- and He-plasmas. This might be caused by the fact that the plasma of GOLEM is not fully ionized and the degree of ionization decreases with the gas pressure. In addition, a systematic increase of the maximum current with U_{CD} is observed for both helium and hydrogen plasmas.

5.4. The Ohmic heating power

The Ohmic heating power is calculated as: $P_{OH} = U_{loop} I_{pl_{max}}$, where U_{loop} is the mean loop voltage averaged over T_{dis} . Ohmic heating power scan is plotted in Fig. 9.

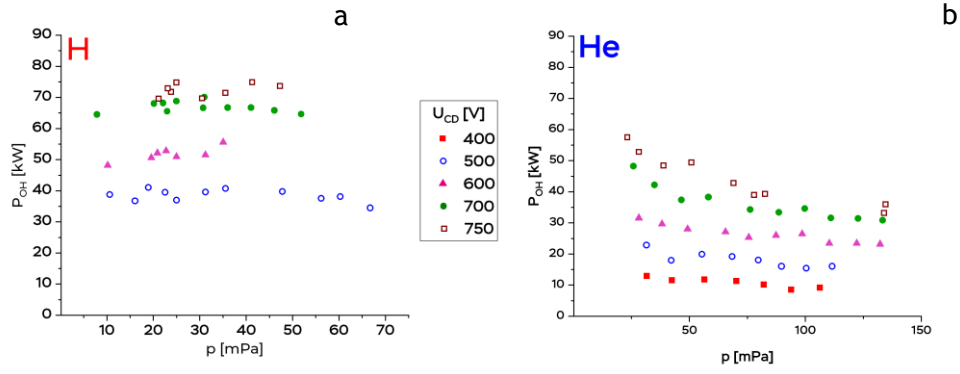


Fig.9. Ohmic heating power versus working gas pressure for hydrogen (a) and helium (b) discharges

Almost no dependence of P_{OH} on the pressure is observed in the both cases. Ohmic heating power in hydrogen plasmas is higher than in helium up to a factor of 2, due to higher maximum plasma current.

5.5. Central electron temperature

The central electron temperature is estimated from Spitzer conductivity as:

$$T_e(0) = 0.0163 \cdot \left(\frac{Z_{eff} I_{pl}}{U_{loop} a^2} \right)^{2/3} \quad [\text{eV, m, m, kA, V}]$$

where a is minor plasma radius and Z_{eff} is effective plasma charge. We estimate $Z_{eff} = 4$ for helium, and $Z_{eff} = 2.5$ for hydrogen plasmas. For $T_e(0)$ estimations the plasma minor radius was calculated using the data of the plasma vertical and horizontal shifts, see eqs in Section 3.1. Fig. 8 shows the estimates for $T_e(0)$ taken for maximum plasma current.

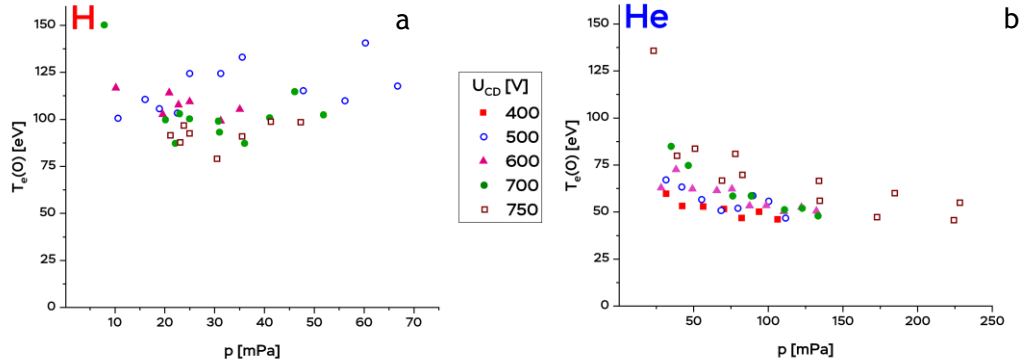


Figure 10. Dependence of the central electron temperature on the pressure for different current drive voltage in hydrogen (a) and helium (b) discharges

Figure 10 shows that in hydrogen plasmas $T_e(0)$ is a factor of 1.5 larger due to larger $I_{pl_{max}}$. Helium plasma shows the systematic decay of the $I_{pl_{max}}$ with initial gas pressure, which is not the case for hydrogen plasma, where the dependence is not clear.

5.6. Electron temperature at the plasma edge

Edge electron temperature $T_e(a)$ was measured by electric probes as shown in section 3.2. Figure 11 shows time-traces of $T_e(a)$ indicating that it tends to reduce with the increase of the initial gas pressure for both hydrogen and helium plasmas.

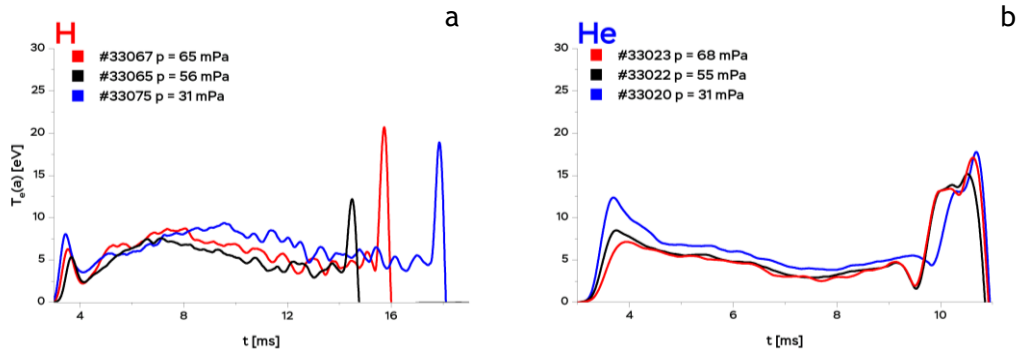


Figure 11. Time evolution of the edge electron temperature for hydrogen and helium plasmas, as measured by Langmuir probe for shots with $U_{CD} = 500V$

The absolute values of the edge temperatures happen to be close for hydrogen and helium plasmas, having the range of several eV and pronounced dynamics during the discharge. Figure 12 shows that the edge temperature depends on the current drive voltage.

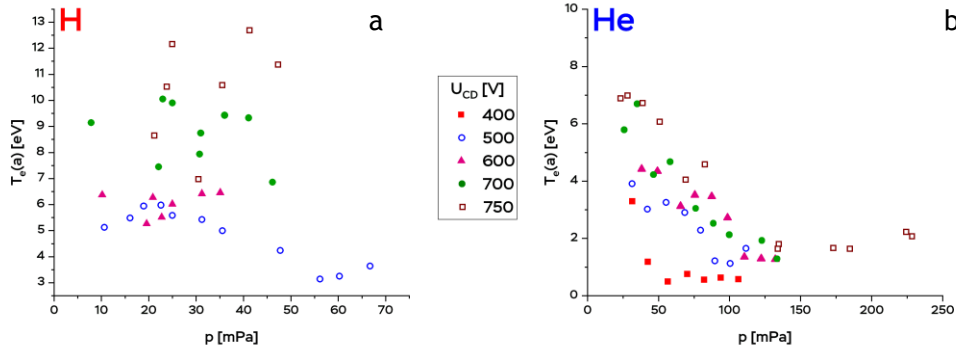


Figure 12. Edge electron temperature dependencies on initial gas pressure and current drive voltage at the moment of maximum plasma current in (a) hydrogen (b) helium discharge

As far as helium mass is four times and charge is two times larger than hydrogen, radiative losses from helium plasma is larger. This explains the lower electron temperature in He plasmas compared to H one in both core (figure 10) and edge (figure 12). The current drive voltage directly affects the plasma current. As GOLEM has only ohmic heating, the current (or U_{CD}) increase leads to an increase of the edge electron temperature, as shown in the fig 12 and core electron temperature, as shown in the fig 10.

Figure 13 presents the edge electron temperature as a function of plasma current. The major trend is clear: the higher is the current the higher is the edge electron temperature. This tendency is in line with the expectation for the ohmic heated plasmas with a plasma current as the only source of thermal energy.

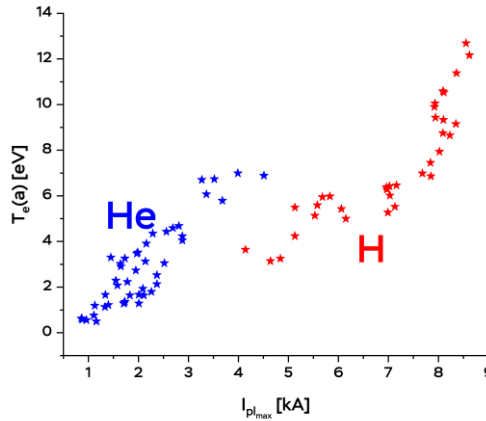


Figure 13. Edge electron temperature versus maximum plasma current for all set of discharges with various current drive voltage U_{CD} . The edge electron temperatures were taken at the moment of maximum plasma current. Combined data for various U_{CD}

Interestingly, for the interval of current overlapping for hydrogen and helium plasmas ($4 \text{ kA} < I_{pl,max} < 5 \text{ kA}$), edge electron temperature for helium plasmas is substantially (for a factor of 2) higher, than for hydrogen plasmas.

5.7. Electron energy confinement time analysis

The global energy confinement time τ_E is defined as

$$\tau_e = \frac{W_e}{P_{OH}} \quad [s, J, W]$$

Where $W_e = \int_{V_p} n_e T_e d^3x$ is the total energy in the plasma column of the volume $V_p = 2\pi^2 R a^2$. Determination of W_e requires knowledge of radial profiles of $T_e(r)$ and $n_e(r)$, which are not measured at GOLEM. To describe scaling of τ_E on measurable quantities, in particular on the pressure of the gas $p = k_B n_e T_{gas}$ (we are limiting n_e as for fully ionized plasma provided by injected gas with temperature T_{gas}), we approximate $W_e = \frac{3}{8} T_e(0) n_e V_p$ (where $3/2$ comes from degrees of freedom and $1/4$ comes from averaging $\langle n_e T_e \rangle$) [27]. Therefore, the electron energy confinement τ_e^{exp} scales with the pressure as (a , $T_e(0)$ and U_{loop} are taken at moment of $I_{pl,max}$):

$$\tau_e^{exp} = \frac{6\pi^2 R}{8k_B T_{gas}} \frac{a^2 T_e(0) p}{U_{loop} I_{pl,max}} \quad [s; m; m^2; K; Pa; K; V; A]$$

τ_e dependence on the gas pressure for helium and hydrogen plasmas is shown in figure 14.

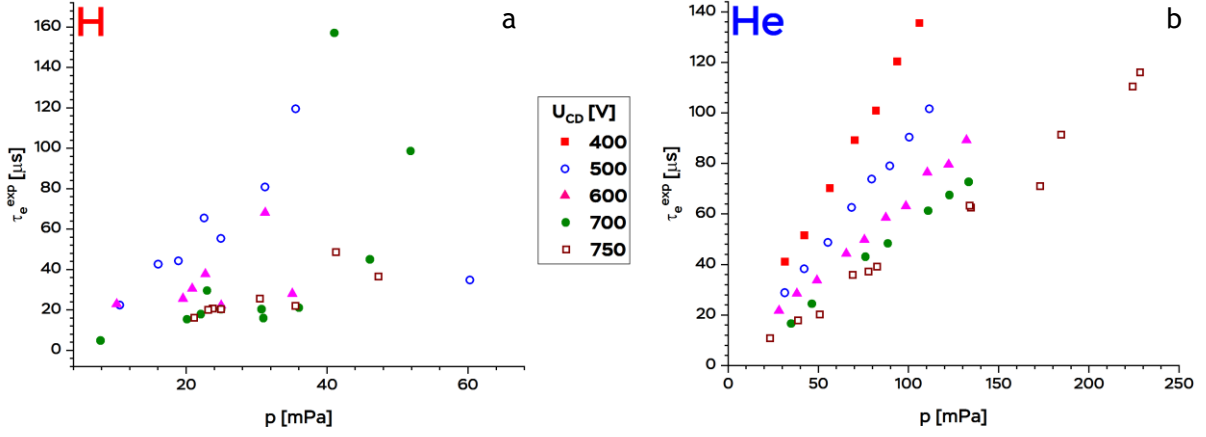


Figure 14: Global electron energy confinement time versus initial gas pressure for hydrogen and helium discharges

We observe a linear increase of τ_E with the pressure (density) in both cases. A clear inverse dependency of τ_E on the U_{CD} is more pronounced for helium shots, which implies a dependency on the plasma current.

It is interesting to compare our data with existing scaling of the global energy confinement time [28], where results from a number of experimental devices were compiled, and an overall scaling law for ohmically heated tokamaks was deduced:

$$\tau_e \sim n_e a^2 \sqrt{q} \quad [s; m^{-3}, m^2]$$

Alternatively, Neo-Alcator scaling was proposed [29]:

$$\tau_e = 1.92 \cdot 10^{-21} \cdot R^{2.04} a^{1.04} n_e \quad [s; m, m, m^{-3}]$$

Scaling law of electron energy confinement time on GOLEM was found as [30]:

$$\tau_e^{GOLEM} = 3 \cdot 10^{-22} \cdot I_p^{0.95} \cdot B_t^{0.31} \cdot P_{OH}^{-1.33} \cdot n_e^{1.04} \quad [s; A, T, W, m^{-3}]$$

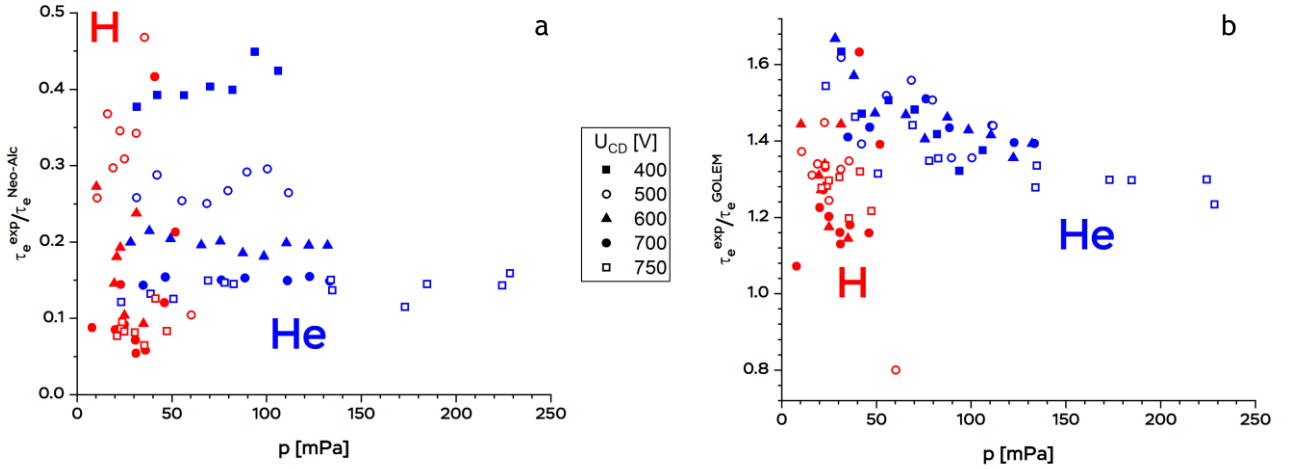


Figure 15: Experimental and Neo-Alcator τ_e -scaling dependence on gas pressure (left) and experimental and GOLEM τ_e -scaling dependence (right)

Figure 15 shows that obtained regimes have about factor of 1.4 better confinement than prediction of the conventional GOLEM scaling for helium, while for hydrogen this factor is slightly lower, about 1.3. On the other hand, for both hydrogen and helium confinement on GOLEM is lower than prediction Neo-Alcator scaling, based on the larger scale tokamaks.

5.8. Displacement of the plasma column and the edge safety factor

Plasma position in the GOLEM tokamak is not controlled by any external vertical/horizontal magnetic fields and evolves spontaneously during a discharge. Therefore, plasma column may not be ideally centered during the discharge. The displacement of the plasma column was routinely derived for by means of Mirnov Coils. A typical temporal evolution of the radial and vertical displacement is shown in fig. 16.

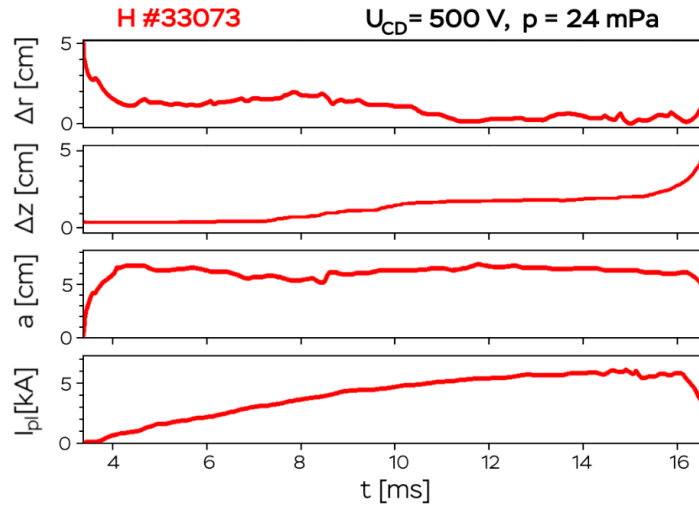


Figure 16. Temporal evolutions of the radial (a), and vertical (b) displacement of the plasma column, resulting plasma minor radius (c) and plasma current (d)

The radial displacement Δr tends to reduce from a few cm up to zero, so plasma column moves inward during the discharge. This is in contrast with the usual picture of toroidal discharges in other tokamaks, where $\Delta r > 0$ due to the Ampere force and increase of plasma pressure (ballooning effect). The possible reason of such behavior of GOLEM plasmas can be a dominant attractive force of the iron core transformer.

In addition, we observe a positive displacement of plasma in the vertical direction Δz during a discharge. The possible reason can be stray radial magnetic field, for example produced by misalignment of the toroidal field coils, which grows up during the discharge.

To compare displacements Δr , Δz over all considered discharges we take the maximum current time as a reference. Δr and Δz were averaged over $20 \mu\text{s}$ around the maximum plasma current. Their dependencies on the working gas pressure are plotted in fig.17.

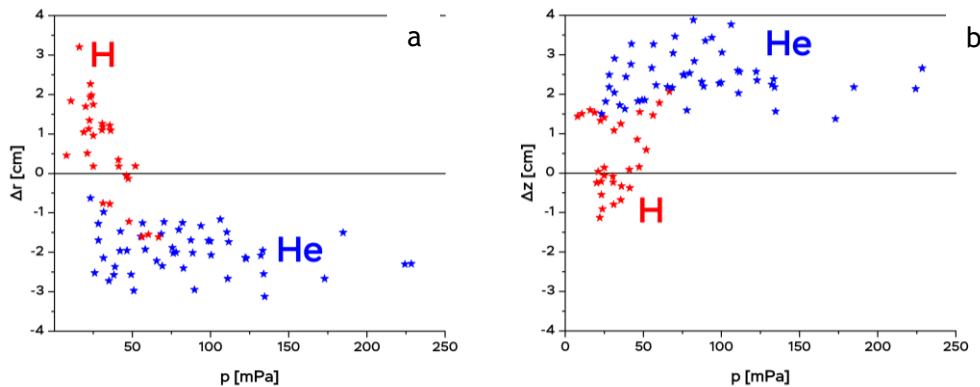


Figure 17. Pressure scans for plasma displacement, (a) – horizontal, (b) – vertical. Combined data for various U_{CD}

It is clearly seen that the displacements are independent on pressure for helium plasmas, while for hydrogen plasma the trend is not pronounced. Helium plasma column is always located inwards by ~ 2 cm and upwards by ~ 2 cm. The scan of displacements over the maximum plasma current is shown in fig. 18.

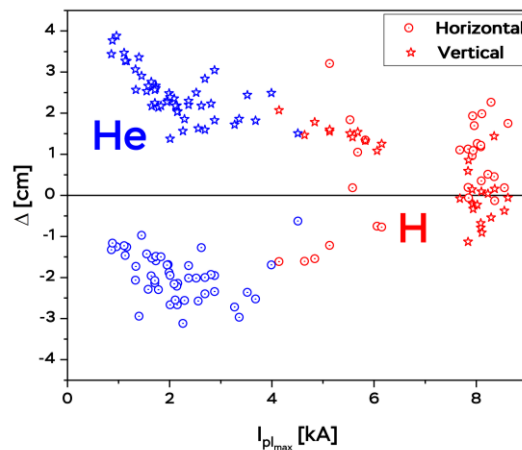


Figure 18. Plasmas displacement versus current. Combined data for various U_{CD}

Plasma current position becomes more downward and inward shifted for helium shots, which is not the case for hydrogen shots. Hydrogen plasmas have a tendency for more central location. The general trend is the more centered column with the increase of the plasma current, the central position is reached in hydrogen plasma.

5.9. Maximum available magnetic flux through the iron core transformer of GOLEM

The iron core transformer of GOLEM is designed to transport the maximum magnetic flux around $\Phi_{\max} = 120$ mWb [25]. The magnetic flux Φ through the central column of the GOLEM transformer can be calculated as the integral of the loop voltage

$$\Phi(t) = \int_0^t U_{\text{loop}}(\tau) d\tau \quad [\text{Wb}, \text{V}, \text{s}]$$

An example of temporal evolution of the loop voltage and resulting magnetic flux $\Phi(t)$ is plotted in fig. 19.

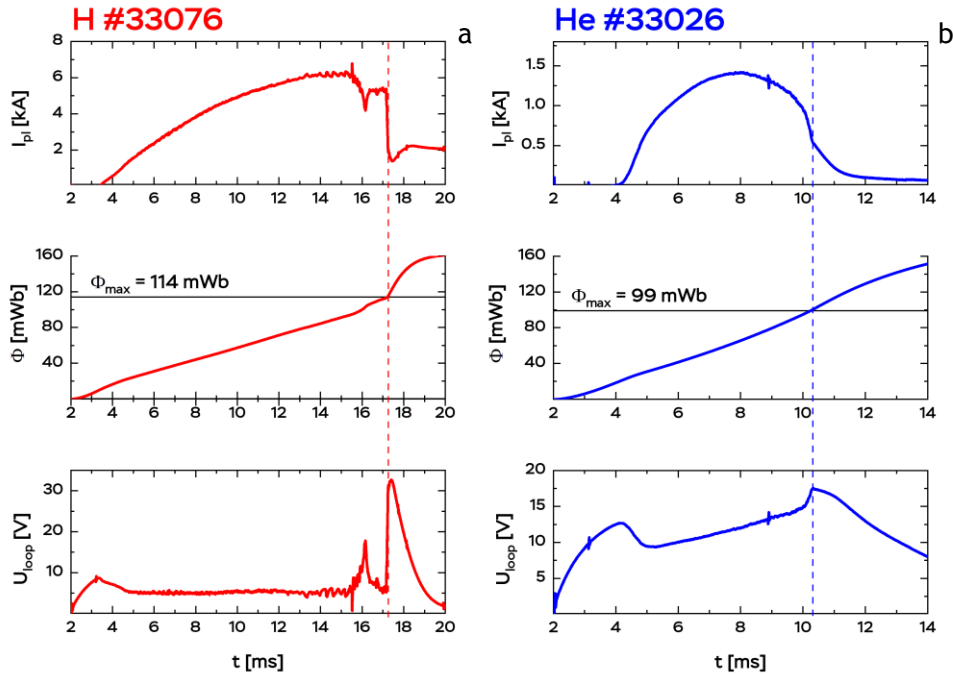


Fig. 19. Evolution of the plasma current, total magnetic flux and loop voltage for H- (a) and He-discharges (b) at $U_{\text{CD}} = 500$ V

We see that discharges are terminated when the magnetic flux through the transformer reaches its designed maximum. It is evident that the duration is inversely proportional to the loop voltage during the plasma phase, i.e. the lower loop voltage at the breakdown time is followed by a longer discharge. The loop voltage is proportional to the effective plasma charge Z_{eff} , which is higher for helium plasmas. This is the reason why the discharge duration T_{dis} in hydrogen plasmas is always longer than in helium ones. With a long vessel heating and glow discharge cleaning the discharge duration is always longer [20].

Note also that a noticeable magnetic flux (~20 - 25%) is already consumed before the breakdown, which shows an importance of optimization of the breakdown conditions for plasma performance.

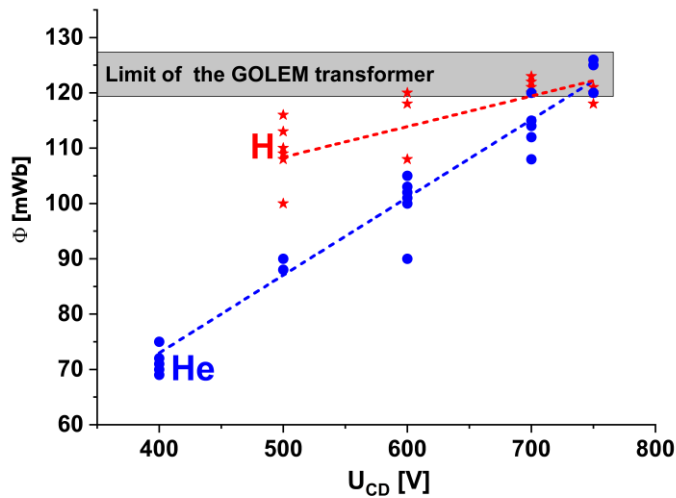


Fig. 20. Maximum magnetic flux versus the charging voltage in hydrogen and helium plasmas

Figure 20 shows the magnetic flux limit of the GOLEM transformer, that is reached only at the highest U_{CD} , in particular in helium plasmas. On the other hand, the discharges at $U_{CD} \leq 500\text{--}600\text{ V}$ are not terminated by a maximum magnetic flux of the transformer, and therefore we have to look for another mechanism, limiting the discharge duration.

5.10. Termination of the discharge by shrinking of plasma column and the decrease of the edge safety factor

The edge safety factor $q(a)$ at the maximum plasma current is:

$$q(a) = \frac{a B_{t_{\max}}}{R_0 B_{p_{\max}}} \sim \frac{a^2 B_{t_{\max}}}{R_0 I_{p1_{\max}}}$$

where $B_{t_{\max}}$ is the toroidal magnetic field at the maximum of the plasma current, plasma minor radius is calculated using the data on the horizontal and vertical displacement (section 5.8).

Taking into account the fact that for a helium plasma, higher current drive voltages correspond to a longer discharge duration (fig.7b), and for a hydrogen series it is not entirely obvious, comparison of the discharge termination process at approximately the same gas pressure and the same current drive voltage should be done.

A possible reason for the discharge termination can be the formation of MHD modes, which can lead to macroscopic instabilities preceding the breakdown. Because of these instabilities, which are noticed in the form of irregular oscillations and then drops in the plasma current, the duration of hydrogen discharges is a kind of random nature due to the inaccuracy of determining the end of the discharge. On the contrary, no magnetic instabilities were observed in helium discharges.

Figure 21 shows the development of a single breakdown of the plasma current, which led to the end of the discharge. This development of events is typical for high gas pressure.

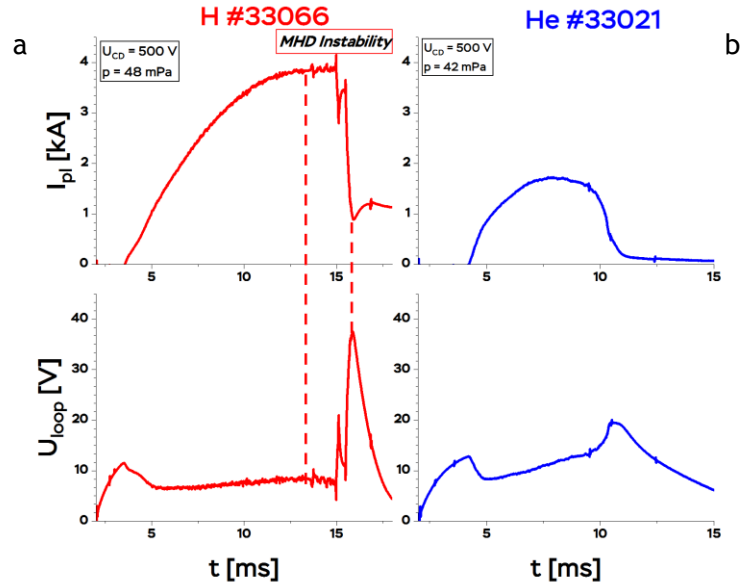


Figure 21. Presence of macroscopic MHD-instability in H- (a) and absence in He-discharges (b)

Here it is possible to determine the value of the safety factor at the plasma boundary $q(a)$ at the moment of this instability. For hydrogen discharges, the minimum $q(a)$ is limited to 2, which indicates that sawtooth oscillations are observed, fig. 22.

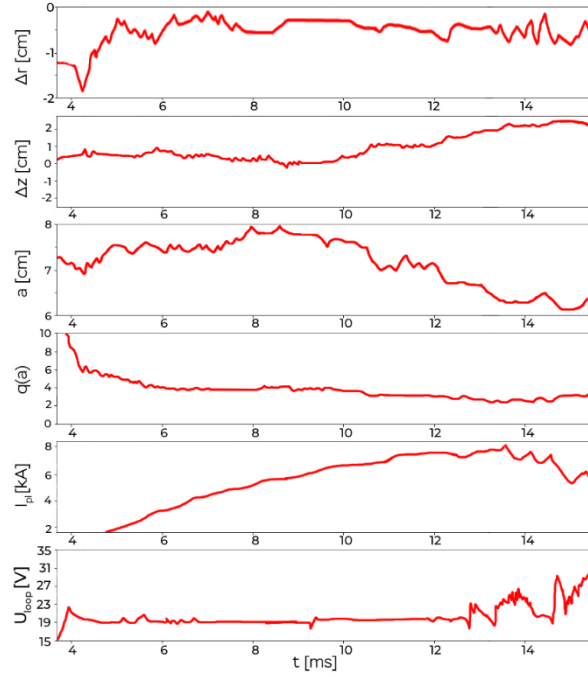


Figure 22. Excitation of MHD instability at the final stage of in hydrogen discharges, when edge safety factor approaches 2, #33093

At the supremum of reached plasma current in helium ($U_{cd} = 750$ V), as well as at the infimum of plasma current in hydrogen ($U_{cd} = 500$ V), some disturbances are observed, which can be identified with weak MHD instability (Fig. 23). Due to the increase in the plasma current and the compression of the plasma column due to a displacement of its axis, the edge safety factor q (a) falls below 2, which leads to the development of MHD instability. For hydrogen, this effect is more notable than for helium.

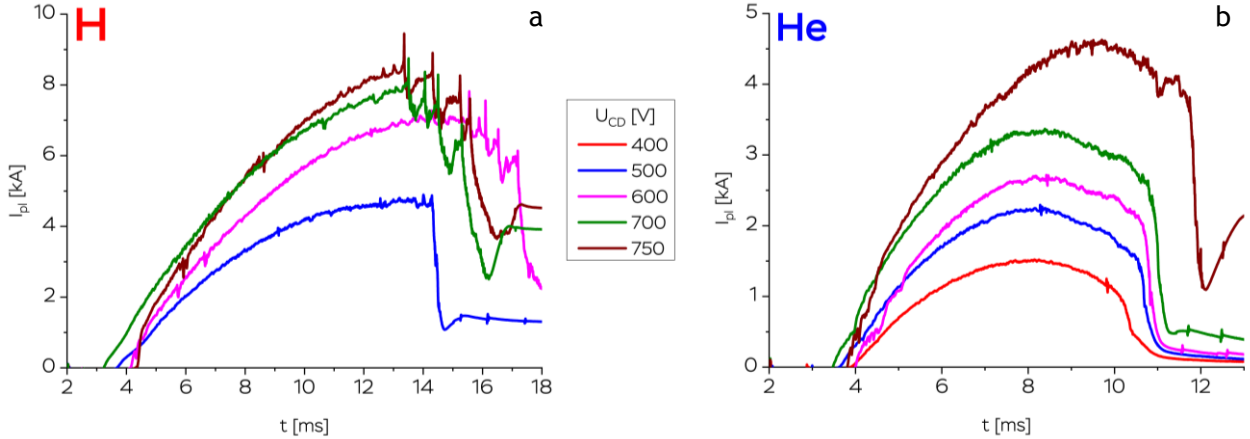


Fig. 23. Evolution of the plasma current in hydrogen (a) and helium (b) plasmas for several charging voltages U_{CD}

5.11. Analysis of magnetic fluctuations measured by Mirnov Coils

Fast Fourier Transform (FFT) technique was used to analyze magnetic oscillations. For the Fourier transform $\mathcal{F}(f)$ of the signals (time series) the power spectrum or power spectral density (PSD) is defined as: $P_{11}(f) = \mathcal{F}(f_1)\mathcal{F}^*(f_1)$ where the asterisk denotes a complex conjugate. For two different signals with $\mathcal{F}_1(f), \mathcal{F}_2(f)$ the cross-spectrum is defined as: $P_{12}(f) = \mathcal{F}(f_1)\mathcal{F}^*(f_2)$. In general, $P_{12}(f)$ is a complex function, so it may be presented as follows:

$$P_{12}(f) = |P_{12}(f)|e^{i\phi_{12}(f)}$$

where $|P_{12}(f)|$ is absolute value of cross-spectrum and $\phi_{12}(f, t) = \arctg\left\{\frac{\text{Im}(P_{12})}{\text{Re}(P_{12})}\right\}$ is cross-phase between two signals.

The coherence between two signals is the normalized cross-spectrum [31]:

$$C_{12}(f) = \frac{|P_{12}(f)|}{\sqrt{P_{11}(f)P_{22}(f)}}$$

An example of power spectrograms for magnetic signals of Mirnov Coils is shown in fig. 24 altogether with plasma current and loop voltage during whole discharge. Time-averaged PSD for chosen time periods is shown near each spectrogram. A coherent fluctuation of magnetic field with the maximum amplitude at $f \sim 25$ kHz is excited from 8 ms up to the appearance of plasma current oscillations at the final stage of the discharge around 13 ms.

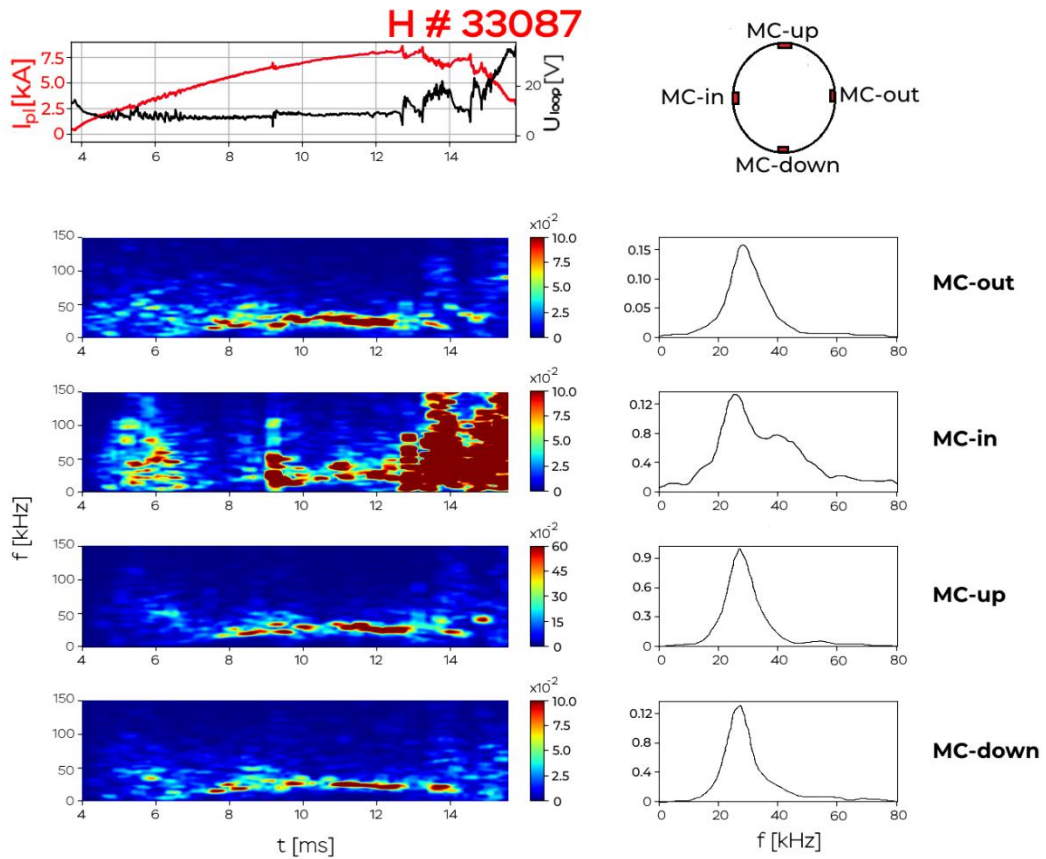


Figure 24. Power spectrograms (left) and time-averaged ($10 \text{ ms} < t < 12.5 \text{ ms}$) power spectra (right) of the Mirnov Coil signals. Coherent magnetic fluctuation is excited in the range 20-40 kHz.

However, left coil MC-in less clearly reproduce such fluctuations, but shows some turbulence at the final stage of the discharge. The results of cross-coherence between MC signals are shown in fig. 25.

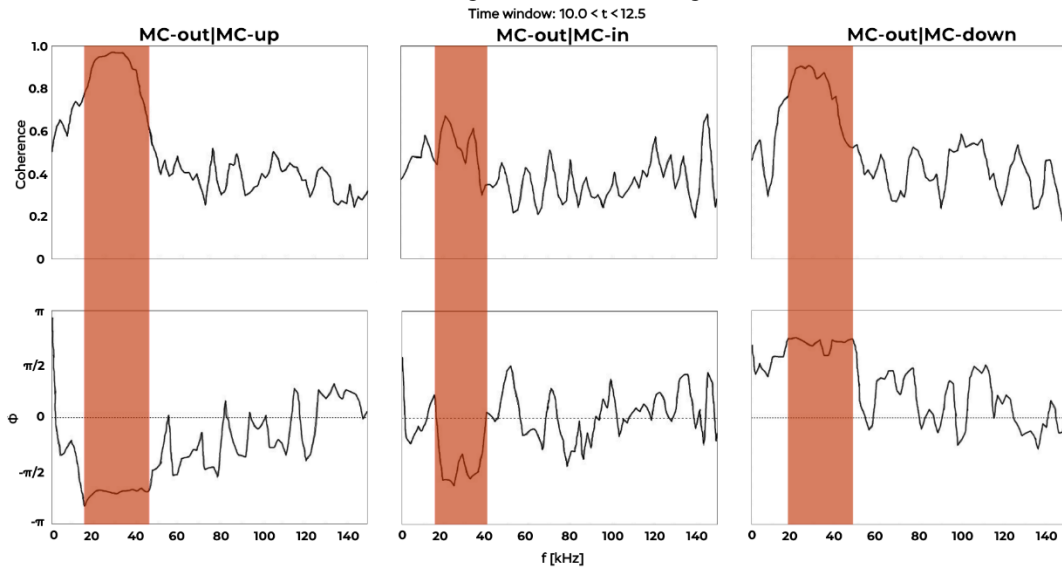


Figure 25. Cross-coherence (top) and cross-phase (bottom) for shot #33087.

Coherent magnetic fluctuation in the range 20-40 kHz has statistically valuable coherence and non-random cross-phase

Top series of graphs shows high coherency at $f \sim 20\text{-}40 \text{ kHz}$ for coil pairs MC-out|MC-up and MC-out|MC-down. The coherence MC-out|MC-in is lower, so only three signals MC-out, MC-up and MC-down were used for poloidal mode number m reconstruction. Cross-phases for each pair of coils represents phase for the second coil in the pair for zero phase in the first coil. Figure 25 shows the following phases for signals:

	MC-out	MC-up	MC-in	MC-down
Phase	0	$-3\pi/4$	$-\pi$	$3\pi/4$
Poloidal angle	0	$\pi/2$	π	$-\pi/2$

that represents the poloidal mode number $m = 3$ for this instability.

In contrast to H-shots the He-shots show a sort of quasi-coherent fluctuations in the range 30-150 kHz, which present a hot topic for plasma research in the medium-size machines [32, 33, 34] as well as in small devices [35, 36, 37]. An example of spectrogram is shown in fig. 26. Figure shows the quiescent period in the phase of the I_{pl} raise (3.6-8 ms), then an appearance of quasi-coherent fluctuations (red curves) in the phase of the I_{pl} decay, and further development of some broadband turbulence at the very end of the discharge (green curves), again, resembling the observations from the medium-size machine [38, 39].

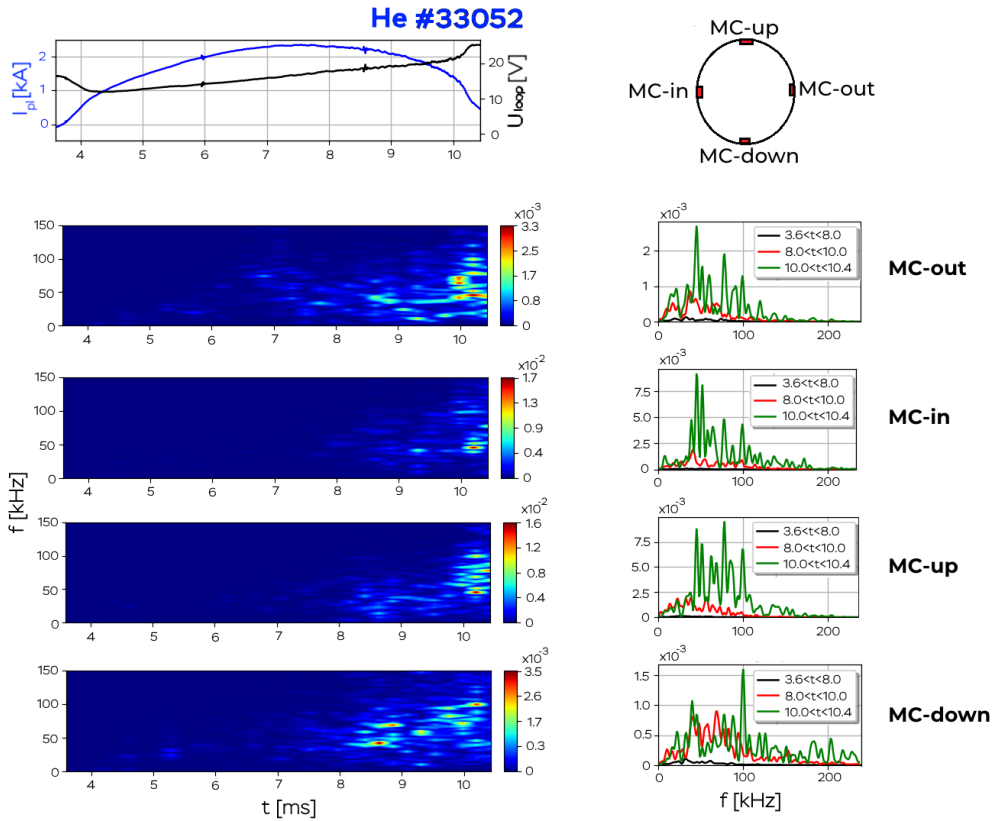


Figure 26. Power spectrograms (left) and time-averaged power spectra (right) of the Mirnov Coil signals. Quasi-coherent magnetic fluctuation is excited in the range 30-150 kHz.

The coherent analysis of the MC data gives the systematic structure of the cross-phase versus frequency in the stage of the I_{pl} decay ($8 \text{ ms} < t < 10 \text{ ms}$), as shown in the cross-phase spectrogram in figure 27a. The cross-phase dependence on frequency shown in figure 27b has linear character. It resembles the direct propagation of broadband ($0 < f < 250 \text{ kHz}$) magnetic perturbation from one probe to another one with a finite velocity. Remarkably, the cross-phase passes through π at 150 kHz and then continue the linear coupling. Note that the increase of the frequency, that passes π , from 120 kHz to 150 kHz indicates the increase in the turbulence rotation during considered time interval.

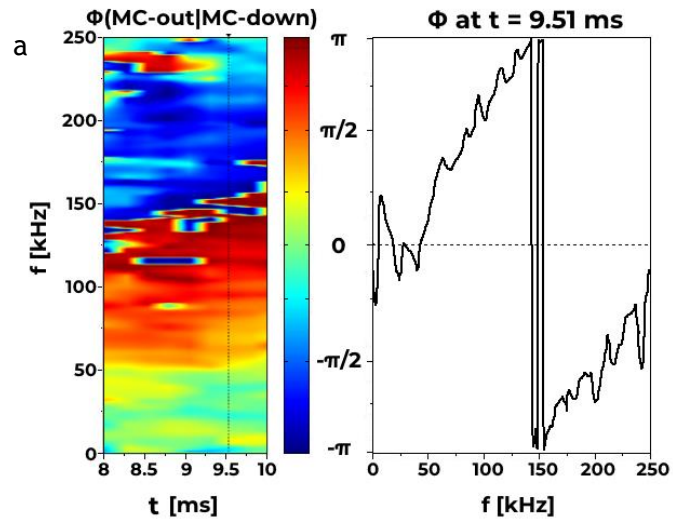


Fig.27. Cross-phase spectrogram of MC-out | MC-down signals (a) and cross-phase spectrum for $t=9.51 \text{ ms}$ (b), shot #33052

a

b

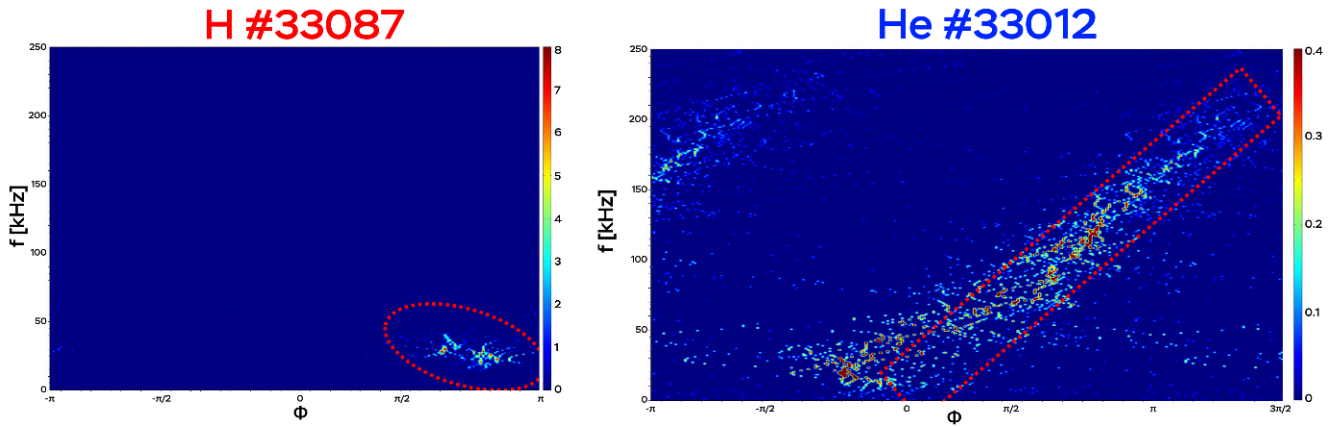


Fig. 28. Two-dimensional power spectra $S(\Phi, f)$ for broadband magnetic turbulence in typical hydrogen (a) and helium (b) discharge

Figure 28 shows two-dimensional frequency-cross-phase power spectra $S(\Phi, f)$ for broadband magnetic turbulence in a typical hydrogen and helium discharges. It shows the coherent magnetic mode with the maximum amplitude at $f \sim 25$ kHz in hydrogen, see fig 26, contrasting with a systematic linear-like structure along the line, starting from the origin $(0, 0)$. The latter indicates the direct propagation of broadband $(0 < f < 250 \text{ kHz})$ magnetic perturbation from one probe to another one. This poloidal propagation might be considered as a poloidal magnetic turbulence rotation with a finite velocity [40].

5.12. Long-range correlations of the edge plasma fluctuations

Long-range correlations indicate any type of global mode of plasma oscillations including Geodesic Acoustic Modes [41]. Electric and magnetic probes in the GOLEM tokamak are located at a distance of a quarter of a torus and at different poloidal angles, see figure 1. Analysis of the coherence and cross-phases between the magnetic oscillations measured by Mirnov Coils and the floating potential oscillations measured by Langmuir probe is shown in fig. 29 and presents a mode with a frequency about 20-40 kHz, clearly visible on all four MCs, in most of hydrogen shots, as coherent magnetic fluctuation, see figs 24 and 25. These fluctuation is observed in the “calm” stage of the discharge, marked by pink ribbon in fig. 29, when the plasma current has not yet reached its maximum and the quenching instabilities typical of a hydrogen discharge have not yet excited. It should be mentioned that the long-range correlations sometimes happen in more extended frequency range 20-60 kHz.

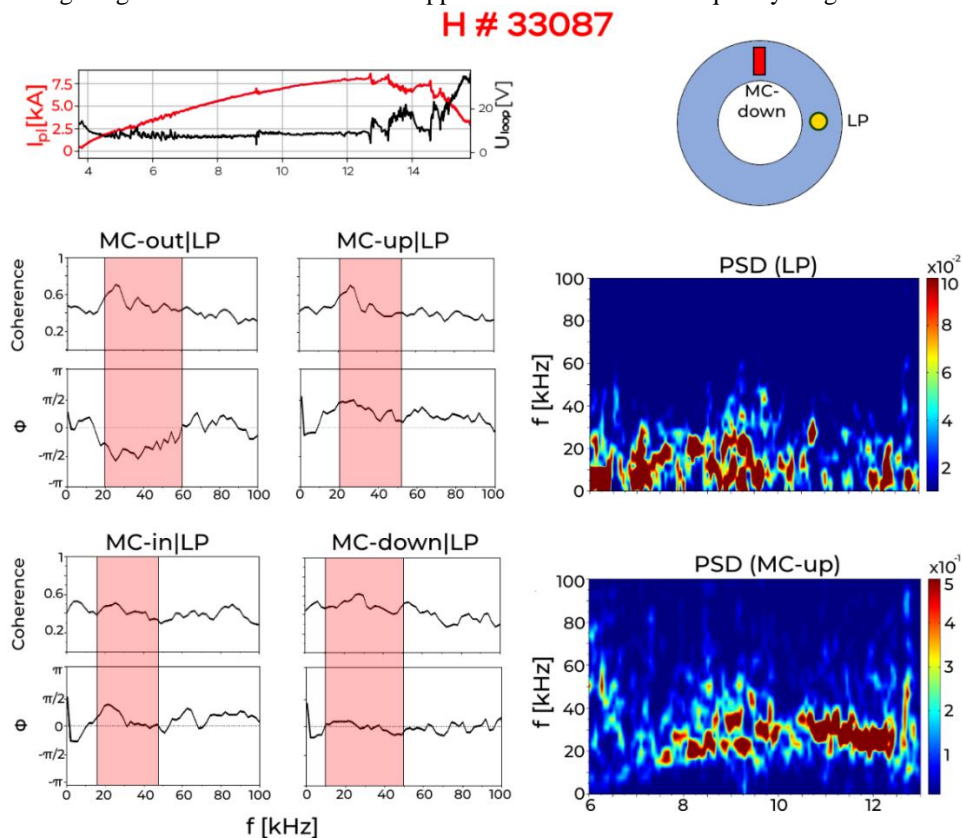


Figure 29. Observation of the long-range correlation for coherent magnetic oscillations. Coherence and cross-phase between plasma potential by Langmuir probe and magnetic oscillations by Mirnov Coils (left) averaged over $6 \text{ ms} < t < 13 \text{ ms}$. The long-range coherence in the range 20-60 kHz exceeds the confidence level of 0.3. Power spectral density of Langmuir probe and one of MCs signals (right).

In contrast to a hydrogen discharge, a helium discharge develops without any noticeable long-range correlations.

6. Summary

Experiments have shown that with the same preset discharge parameters (gas pressure, current drive voltage, magnetic field, etc.) plasma scenarios in hydrogen and in helium in GOLEM are radically different. In hydrogen plasma magnetic instabilities usually occur near the maximum plasma current, that lead to the disruption and plasma termination, while the helium plasma quietly extinguishes by itself due to the exhaust of the magnetic flux in the primary winding of tokamak transformer.

The main links between the plasma discharge parameters were confirmed: the discharge duration and electron temperature increases with plasma current, which in turn increases with gas pressure. In addition, electron energy confinement time happens to exceeded τ_e scaling for GOLEM by a factor of 1.4.

The presence of long-range toroidal/poloidal correlations between electric potential and magnetic perturbation was observed and the existence of broadband magnetic turbulence was shown for the first time.

Acknowledgement

Authors would like to thank Ruslan Begishev, Ivan Emekeev, Mikhail Gorbun and Nikita Vadimov for participating in the experiments. GOLEM operation is supported by IAEA research contract F13019 'Network of Small and Medium Size Magnetic Confinement Fusion Devices for Fusion Research'. MHD turbulence and long-range correlation studies were supported by Russian Science Foundation, project 19-12-00312.

References

- [1] P. Manas, C. Angioni, A. Kappatou et al, The confinement of helium tokamak plasmas, impact of electron heating, turbulent transport and zonal flows 2019 Nucl. Fusion **59** 014002
- [2] R.E.Waltz, R.L. Dewar and X. Garbet, Theory and simulation of rotational shear stabilization of turbulence, 1998 Phys. Plasmas **5** 1784
- [3] G. Van Oost, V.V. Bulanin, A.J.H. Donné, et al, Multi-machine studies of the role of turbulence and electric fields in the establishment of improved confinement in tokamak plasmas, 2007 Plasma Phys. Control. Fusion **49** A29-A44
- [4] M. Nakata, M. Nunami and H. Sugama, Multi-machine studies of the role of turbulence and electric fields in the establishment of improved confinement in tokamak plasmas, 2017 Phys. Rev. Lett. **118** 165002
- [5] M. Gryaznevich, G. Van Oost, P. Peleman, et al, Results of Joint Experiments and other IAEA activities on research using small tokamaks 2009 Nucl. Fusion **49** 104026
- [6] G. Van Oost, J. Adánek, V. Antoni et al, Turbulent transport reduction by E×B velocity shear during edge plasma biasing: recent experimental results 2003 Plasma Phys. Control. Fusion **45** 621-643
- [7] M. Gryaznevich et al, Characteristics of the core and edge plasma turbulence in small Tokamaks 2008 Iranian Physical Journal, 2-3, 1-7
- [8] M.P. Gryaznevich, J. Stöckel, G. Van Oost, et al, Contribution of Joint Experiments on Small Tokamaks in the framework of IAEA Coordinated Research Projects to mainstream Fusion Research 2020 Plasma Sci. Technol. **22** 055102
- [9] G. Van Oost, M. Gryaznevich, E. Del Bosco, et al, Joint Experiments on the Tokamaks CASTOR and T-10, 2008 AIP Conf. Proc. 996, 24
- [10] G. Van Oost, J.P. Gunn, A. Melnikov, et al The Role of Radial Electric Fields in the Tokamaks TEXTOR-94, CASTOR, and T-10 2001 Czechoslovak Journal of Physics, **51**(10) pp. 957-975
- [11] M. Gryaznevich, G Van Oost, J Stöckel, et al, Contribution to Fusion Research from IAEA Coordinated Research Projects and Joint Experiments. 2015 Nucl. Fusion **55** 104019
- [12] A. Fujisawa et al, Experimental progress on zonal flow physics in toroidal plasmas, 2007 Nucl. Fusion **47** S718
- [13] A.V. Melnikov et al, Investigation of the plasma potential oscillations in the range of geodesic acoustic mode frequencies by heavy ion beam probing in tokamaks, 2005 Czech. J. Phys. **55** 349
- [14] A.V. Melnikov et al, Correlation properties of geodesic acoustic modes in the T-10 tokamak, 2015 J. Phys.: Conf. Ser. **591** 012003
- [15] A.V. Melnikov et al, Investigation of geodesic acoustic mode oscillations in the T-10 tokamak, 2006 Plasma Phys. Control. Fusion **48** S87
- [16] A. Fujisawa et al, Identification of zonal flows in a toroidal plasma, 2004 Phys. Rev. Lett. **93** 65002
- [17] J.A. Alonso et al, Observation of oscillatory radial electric field relaxation in a helical plasma, 2017, Phys. Rev. Lett. **118** 185002
- [18] A.V. Melnikov et al, Heavy ion beam probing—diagnostics to study potential and turbulence in toroidal plasmas, 2017, Nucl. Fusion **57** 072004
- [19] A.V. Melnikov et al, ECRH effect on the electric potential and turbulence in the TJ-II stellarator and T-10 tokamak plasmas, 2018, Plasma Phys. Control. Fusion **60** 084008
- [20] V. Svoboda et al, Operational Domain in Hydrogen Plasmas on the GOLEM Tokamak, 2019 Journal of Fusion Energy **38** 253–261
- [21] V. Svoboda, B. Huang, J. Mlynar et al, Multi-mode remote participation on the GOLEM tokamak. 2011 Fusion Eng. Des. **86**, pp.1310–1314
- [22] I.H. Hutchinson, Principles of plasma diagnostics, doi: 10.1017/CBO9780511613630
- [23] J. Adánek et al., Diagnostics of magnetized low temperature plasma by ball-pen probe, 2012 NUKLEONIKA, **57**(2) pp.297–300
- [24] P. Mácha, Měření základních parametrů okrajového plazmatu pomocí kombinované ball-pen a Langmuirovy sondy na tokamaku GOLEM, Bachelor Thesis
- [25] M. Valovic, Convective losses during current initiation in tokamaks, 1987 Nuclear Fusion **27** 599

-
- [26] B. Lloyd, P.G. Carolan and C.D. Warrick, ECRH-assisted start-up in ITER, 1996 Plasma Phys. Control. Fusion, **38** (9) 1627
- [27] J. Brotankova, PhDthesis, <http://golem.fjfi.cvut.cz/wiki/Library/GOLEM/PhDthesis/JanaBrotankovaPhDthesis.pdf>
- [28] R.J. Goldston, ENERGY CONFINEMENT SCALING IN TOKAMAKS: SOME IMPLICATIONS OF RECENT EXPERIMENTS WITH OHMIC AND STRONG AUXILIARY HEATING, PPLR 1984
<https://www.osti.gov/servlets/purl/5208115>
- [29] R.R. Parker, M. Greenwald, S.C. Luckhardt, E.S. Marmor, M. Porkolab, S.M. Wolfe, PROGRESS IN TOKAMAK RESEARCH AT MIT, 1985 https://dspace.mit.edu/bitstream/handle/1721.1/94844/85ja014_full.pdf?sequence=1
- [30] J. Hillaret, <https://clck.ru/ScMwn> (golem/wiki/scaling.png)
- [31] D.E. Smith, E. J. Powers and G. S. Caldwell, Fast-Fourier-Transform Spectral-Analysis Techniques as a Plasma Fluctuation Diagnostic Tool, 1974 IEEE Trans. on Plasma Sci. **2** (4) pp. 261-272
- [32] V.A. Vershkov, D.A. Shelukhin, S.V. Soldatov, et al, Summary of experimental core turbulence characteristics in ohmic and electron cyclotron resonance heated discharges in T-10 tokamak plasmas 2005 Nucl. Fusion **45** (10) S203-S226
- [33] M.A. Drabinskiy, L.G. Eliseev, P.O. Khabanov, et al, Radial structure of quasi-coherent mode in ohmic plasma of the T-10 tokamak 2019 Journal of Phys.: Conf. Series **1383** 012004
- [34] A. Kramer-Flecken et al, Turbulence studies with means of reflectometry at TEXTOR, 2004 Nucl. Fusion **44** 1143
- [35] Yu.K. Kuznetsov, I.C. Nascimento, C. Silva, et al, Long-distance correlations in TCABR biasing experiments 2012 Nucl. Fusion **52** 063004
- [36] A. Malaquias, R.B. Henriques, and I.S. Nedzelsky. Inversion methods for the measurements of mhd-like density fluctuations by heavy ion beam diagnostic. 2015 Journal of Instr. **10**(09) P09024.
- [37] A.V. Melnikov, T. Markovic, L.G. Eliseev, et al, Quasicoherent modes in the COMPASS tokamak 2015 Plasma Phys. and Control. Fusion **57** 065006
- [38] V.A. Vershkov, D.A. Shelukhin, G.F. Subbotin, et al Density fluctuations as an intrinsic mechanism of pressure profile formation 2015 Nucl. Fusion **55** 063014
- [39] V.A. Vershkov, M.A. Buldakov, G.F. Subbotin, et al, 3D structure of density fluctuations in the T-10 tokamak and new approach for current profile estimation 2019 Nucl. Fusion **59** (6) 066021
- [40] L. Eliseev, A. Melnikov, S. Perfilov, et al, Two point correlation technique for the measurements of poloidal plasma rotation by Heavy Ion Beam Probe 2012 Plasma and Fusion Research **7** 2402064
- [41] D. Basu et al Geodesic acoustic mode (GAM) like oscillations and RMP effect in the STOR-M tokamak 2018 Nucl. Fusion **58** 024001